High-Resolution MR Imaging of Muscular Fat Fraction—Comparison of Three T_2-Based Methods and Chemical Shift-Encoded Imaging

Lena Trinh[1], Emelie Lind[1,2], Pernilla Peterson[1], Jonas Svensson[1,3], Lars E. Olsson[1], and Sven Månsson[1]

[1]Medical Radiation Physics, Department of Translational Medicine, Lund University, Skåne University Hospital, Malmö, Sweden; [2]Department of Medical Radiation Physics, Lund University, Lund, Sweden; [3]Medical Imaging and Physiology, Skåne University Hospital, Lund, Sweden

Corresponding Author:
Lena Trinh, MSc
Medical Radiation Physics, Inga Marie Nilssons gata 49, Skåne University Hospital, SE-205 02 Malmö, Sweden;
E-mail: lena.trinh@med.lu.se

Key Words: fat quantification, Bayesian probability theory, non-linear least squares, T_2, high-resolution imaging

Abbreviations: Chemical shift-encoded imaging (CSEI); fat fraction (FF); magnetic resonance imaging (MRI); non-linear least squares (NLLS); multi echo gradient echo (MGRE); repetition time (TR); echo time (TE); bandwidth (BW); multi echo spin echo (MESE); T_2-relaxation time of fat ($T_{2,f}$); T_2-relaxation time of water ($T_{2,w}$); region-of-interest (ROI); signal-to-noise ratio (SNR)

ABSTRACT

Chemical shift-encoded imaging (CSEI) is the most common magnetic resonance imaging fat–water separation method. However, when high spatial resolution fat fraction (FF) images are desired, CSEI might be challenging owing to the increased interecho spacing. Here, 3 T_2-based methods have been assessed as alternative methods for obtaining high-resolution FF images. Images from the calf of 10 healthy volunteers were acquired; FF maps were then estimated using 3 T_2-based methods (2- and 3-parameter nonlinear least squares fit and a Bayesian probability method) and CSEI for reference. In addition, simulations were conducted to characterize the performance of various methods. Here, all T_2-based methods resulted in qualitatively improved high-resolution FF images compared with high-resolution CSEI. The 2-parameter fit showed best quantitative agreement to low-resolution CSEI, even at low FF. The estimated T_2-values of fat and water, and the estimated muscle FF of the calf, agreed well with previously published data. In conclusion, T_2-based methods can provide improved high-resolution FF images of the calf compared with the CSEI method.

INTRODUCTION

Chemical shift-encoded imaging (CSEI) is a common quantitative magnetic resonance imaging (MRI) method for fat–water separation and measurement of fat content in numerous body parts, such as the liver and skeletal muscles (1–5). In skeletal muscles, fatty infiltration has been related to, for example, insulin resistance and various neuromuscular diseases (6–11). The location of fat accumulation within the muscle has also been shown to be important (6), as some muscle groups are more likely to accumulate fat (12). Depending on the muscle group involvement, the outcome of some neuromuscular diseases can show a large variability (11, 13). In addition, different neuromuscular diseases show different fat infiltration patterns of the muscle groups. By detecting these patterns, it might be easier to identify a specific disease (11, 14). To enable and simplify the distinction between the different muscle groups, and between inter- and intramuscular fat, high-resolution fat fraction (FF) images are desirable. CSEI is a validated method for fat quantification purposes (4, 15), and it has previously been used for skeletal muscle applications (1, 2, 5).

Previously, fat quantification methods based on differences in fat and water T_2 (16) rather than chemical shifts have been suggested for applications in skeletal muscles (17, 18). With T_2-based methods, there is a possibility of obtaining information on FF and T_2 relaxation times simultaneously (18). This would offer more information about the status of the disease, as a change in muscle T_2-relaxation time has been shown to reflect the activity and progress of neuromuscular diseases (13, 19), complementing the information about the fat infiltration degree that primarily serves as a severity indicator (14). Moreover, there are several challenges associated with the CSEI technique, particularly when high resolution is required, which may be addressed by using T_2-based methods. For example, increasing the resolution increases the minimal achievable interecho time which may have a negative impact on the CSEI fat quantification accuracy (20). In addition, it is common that fat/water swaps are present in FF images when using CSEI.

To obtain both the amplitudes and the T_2-relaxation times of the fat, as well as the water component of the signal, a nonlinear least squares (NLLS) fitting method is commonly used (21, 22). However, NLLS has known problems with estimating the parameters correctly when 1 component is considerably larger than the other (23, 24). As a consequence, it may be difficult to measure low FFs using NLLS. In such cases, a fitting method based on Bayesian probability theory could be an alternative, as it has also been shown to be more robust against noise

© 2017 The Authors. Published by Grapho Publications, LLC This is an open access article under the CC BY-NC-ND license (http://creativecommons.org/licenses/by-nc-nd/4.0/).
ISSN 2379-1381 http://dx.doi.org/10.18383/j.tom.2017.00011

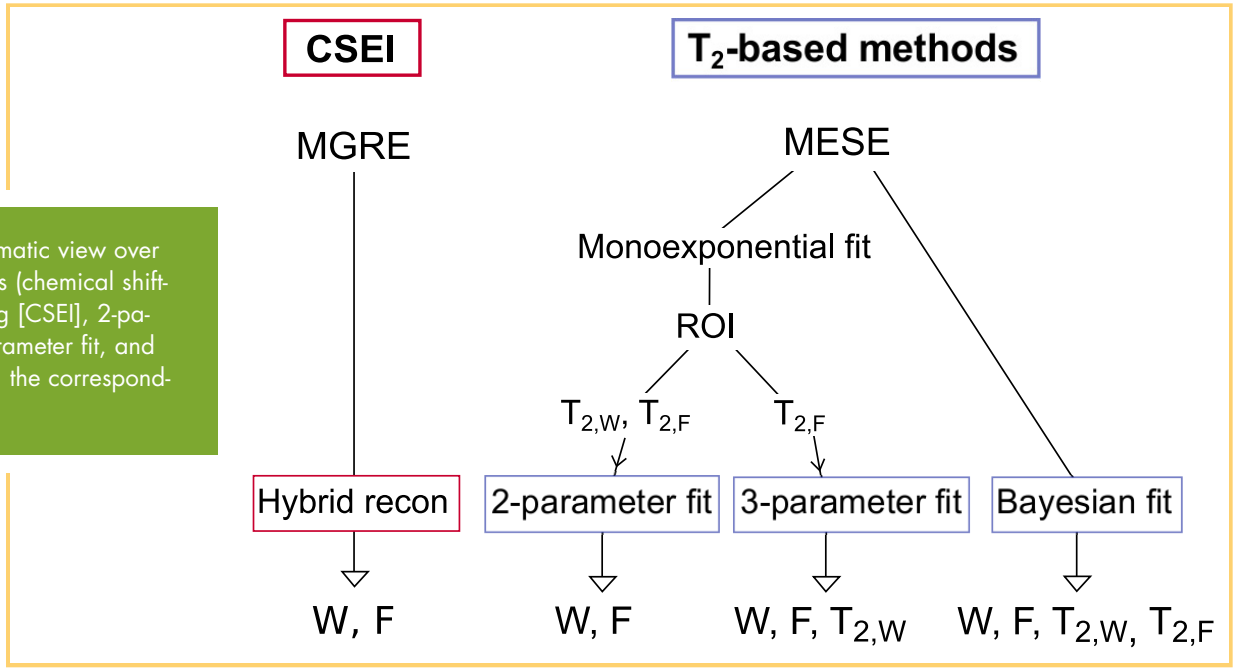

Figure 1. Schematic view over the used methods (chemical shift-encoded imaging [CSEI], 2-parameter fit, 3-parameter fit, and Bayesian fit) and the corresponding outputs.

compared with NLLS (25). Bayesian fitting models have been proposed for other MRI applications such as intra-voxel incoherent motion imaging (26) and myelin water fraction estimations (27), but have, to the best of our knowledge, not yet been evaluated for fat quantification purposes.

The aim of this study was to examine the accuracy and noise performance of 3 different T_2-based fat quantification methods, using high-resolution MRI for low FFs in healthy volunteers, and compare it with CSEI. The first T_2-based method uses fixed T_2-relaxation times of both water and fat as described by Kan et al. (17). The second method uses only a fixed fat T_2-relaxation time to study the possibility of obtaining a simultaneous T_2 map of water. The third method is based on Bayesian probability theory as described by Barbieri et al. (26), in which neither relaxation time is fixed. In this study, the muscular FF was measured in the calf of healthy volunteers, and simulations were made to study possible biases in the estimation of the FF using the T_2-based methods.

METHODOLOGY

Subjects

In total, 10 healthy volunteers, 3 males (mean age, 28 years; range 25–30 years) and 7 females (mean age, 28 years; range, 24–32 years), were recruited and scanned with the approval from the regional ethical board. Informed consent was obtained from all volunteers.

MRI Data Acquisition

All measurements were acquired using a 3 T scanner (MAGNETOM Trio, Siemens Healthineers, Erlangen, Germany) and a 6-element body matrix coil. All data were obtained at 2 matrix sizes, 128×128 and 512×512, keeping the field of view constant at 280×280 mm^2 and thus acquiring data at low- and high-spatial resolution. A single 6-mm transversal slice was collected for each acquisition, centered at the widest part of the left calf of each volunteer.

A multi-echo gradient echo (MGRE) sequence with 6 echoes was used for the CSEI method. To avoid T_1 bias, a long repetition time (TR = 500 milliseconds) and a small flip angle (12°) were used. By estimating the number of signal averages as a function of interecho spacing, echo times (TEs) were chosen to obtain as small interecho spacing for the highest number of signal averages value as possible. The bandwidth (BW) was then set as low as possible without affecting the interecho time. In this way, a minimal interecho time with a high noise performance was ensured. With the first TE set to the shortest possible, the following parameters were used: $TE_1/\Delta TE$ = 1.11/1.56 milliseconds (low resolution), $TE_1/\Delta TE$ = 2.57/3.92 milliseconds (high resolution), BW = 1776 Hz/px (low resolution), and BW = 651 Hz/px (high resolution). Acquiring 1 average, the scanning times were 1 minute 6 seconds (low resolution) and 4 minutes 18 seconds (high resolution). From 1 subject, additional high-resolution CSEI images were collected with 2, 3, and 9 averages that had scanning times of 8 minutes 34 seconds, 12 minutes 50 seconds, and 38 minutes 29 seconds, respectively.

For the T_2-based methods, 32 multi-echo spin echo (MESE) images were acquired with a 180° refocusing pulse and the following settings: TR = 2000 milliseconds, ΔTE = 9.2 milliseconds (low and high resolution), BW = 425 Hz/px (low resolution), BW = 391 Hz/px (high resolution), and number of averages = 1. To avoid long acquisition times, parallel imaging (GRAPPA) was used with an acceleration factor of 2. The resulting scan times were 2 minutes 36 seconds (low resolution) and 9 minutes (high resolution).

Fat/Water-Separation Methods

The methods used in this study are summarized in Figure 1. All calculations were performed using MATLAB (r2017a, The MathWorks, Inc., Natick, MA).

Chemical Shift-Encoded Imaging

The FF was calculated using a complex and magnitude-based iterative multiecho water–fat separation algorithm (28), with a

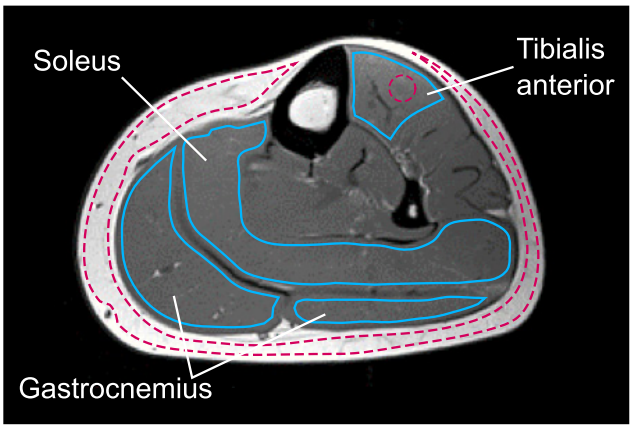

Figure 2. The regions of interest (ROIs) used for calculating $T_{2,W}$ and $T_{2,F}$ (dashed line), and the fat fraction (FF) in 3 calf muscles (solid line): gastrocnemius, soleus, and tibialis anterior.

multipeak fat model (29) and a joint T_2^* estimation (30). Using 6 echoes (30), the FF was calculated using the following equation:

$$Fat\ fraction = 100 \cdot real\left(\frac{F}{W+F}\right) \quad (1)$$

where the complex-valued F and W are the estimated fat and water signals, respectively. T_1 bias was avoided by using a low flip angle acquisition.

T_2-Relaxation Time-Based Imaging

Two of the T_2-based methods use a fixed T_2-relaxation time of fat ($T_{2,F}$), of which 1 uses a fixed T_2-relaxation time of water ($T_{2,W}$) as well. To obtain these values, a monoexponential fit of the signal decay was carried out voxel by voxel, resulting in a T_2 map. For each volunteer, individual $T_{2,F}$ and $T_{2,W}$ values were then calculated as the mean value within corresponding regions of interest (ROIs), which were drawn in subcutaneous fat and muscle tissue, respectively (Figure 2). The ROI of fat was drawn to include as much of the subcutaneous fat as possible, avoiding visible blood vessels. In 1 volunteer, the subcutaneous fat layer was too thin for ROI definition. For this volunteer, the mean $T_{2,F}$ of the rest of the volunteers was calculated and used instead. The muscle ROI was drawn in a small part of tibialis anterior without any visible fat to minimize fat bias in the estimation of $T_{2,W}$. Echoes 2–16 were used for all estimations using MESE data. The first echo was excluded owing to stimulated echo effects present in all other echoes, whereas the last echoes were excluded to reduce noise bias.

Two-Parameter Fit–Fixed $T_{2,F}$ *and* $T_{2,W}$. Using the estimated $T_{2,F}$ and $T_{2,W}$ values from the monoexponential fit, the amplitudes of water W and fat F could be calculated by a simple linear regression, as described by Kan et al. (17). The signal model is given by using the following equation:

$$S(t) = We^{-\frac{t}{T_{2,W}}} + Fe^{-\frac{t}{T_{2,F}}} \quad (2)$$

where S is the measured signal at TE t, and $T_{2,F}$ and $T_{2,W}$ are kept fixed.

Three-Parameter Fit–Fixed $T_{2,F}$. Using the same signal model [equation (2)] as in the 2-parameter fit and fixed $T_{2,F}$ value, $T_{2,W}$, W, and F were estimated using a trust region-based NLLS fitting algorithm.

Bayesian Fitting Method. An alternative to exponential fitting is using a Bayesian probability method (31). Here, all four parameters ($T_{2,W}$, $T_{2,F}$, W, and F) are estimated simultaneously using the method described by Barbieri et al. (26) using the MATLAB function *slicesample*. The signal model is given by the following equation:

$$S = S_0\left((1-f)e^{-\frac{t}{T_{2,W}}} + fe^{-\frac{t}{T_{2,F}}}\right) \quad (3)$$

where S_0 denotes the signal at $t = 0$ and f denotes the FF in the range [0, 1]. To obtain S_0, linear regression was performed on linearized data, $\ln(S)$, in each voxel. However, owing to the biexponential form of the signal decay, $\ln(S)$ is not linear. To compensate for this, $\ln(S)$ was weighted by the signal amplitude S, making the fit rely mostly on the earlier echoes of the signal. Water and fat amplitudes, $W = S_0(1-f)$ and $F = S_0 f$, respectively, were calculated before correcting for T_1 bias and calculating FF as described by equation (4).

Fat Fraction Calculation and T_1-Correction

Owing to the long T_1-relaxation time of muscle tissue and the desire to keep the acquisition times feasibly low, all the T_2-based fat quantification methods described in the above sections were corrected for T_1-relaxation bias. The T_1-relaxation times $T_{1,W}$ = 1420 milliseconds and $T_{1,F}$ = 371 milliseconds (16) were used to correct the water and fat signal amplitudes according to $F_{T1corr} = F/[1-\exp(-TR/T_{1,F})]$ and $W_{T1corr} = W/[1-\exp(-TR/T_{1,W})]$, respectively. Hence, the FF can be described using the following equation:

$$Fat\ Fraction = 100 \cdot \frac{F_{T1corr}}{W_{T1corr} + F_{T1corr}}. \quad (4)$$

Because the MGRE data were collected with a low flip angle, no correction for T_1 bias was needed for CSEI.

Data Analysis

To compare the 4 methods, 3 ROIs were drawn in the calf muscles of all 10 volunteers following the outlines of tibialis anterior, soleus, and gastrocnemius (Figure 2). Small areas with fat–water swaps in the high-resolution FF images calculated with CSEI were excluded from the ROIs. If the fat–water swap extended over a large area covering most of the muscle such that no swap-free ROI could be defined, the entire muscle group was excluded from further analysis.

Mean signal-to-noise ratios (SNRs) of the collected MGRE and MESE magnitude images were calculated as $SNR = 0.655 \cdot S/\sigma$ where 0.655 is due to the Rayleigh distribution of the noise in magnitude images (32) and σ is the standard deviation of the background noise. The SNR of both subcutaneous fat and muscle tissue was calculated. To calculate the standard deviation of the background noise of the MESE data, the ROIs were placed near the edge of the images where the g-factor was expected to be close to 1.

Wilcoxon signed-rank tests and Bland–Altman analysis were performed to compare the estimated FFs within the ROIs

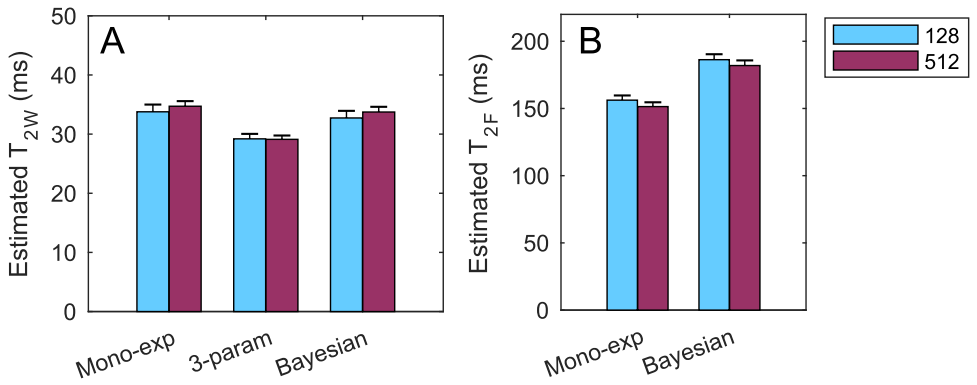

Figure 3. The mean and standard deviation of $T_{2,W}$ (A) within an ROI placed in tibialis anterior and $T_{2,F}$ (B) within an ROI placed in the subcutaneous fat, of all volunteers (except one in the mono-exponential fit) at high- and low-resolution imaging.

using the 2-parameter fit, 3-parameter fit, Bayesian fit, and high-resolution CSEI, to the FFs calculated with low-resolution CSEI.

Simulations

Simulations were conducted to investigate the effects of incorrect T_2 estimations, of incorrect signal amplitude, and of noise on the calculated FF. In all simulations, a biexponential model [equation (2)] was used to describe the signal decay using $T_{2,W}$ = 40 milliseconds and $T_{2,F}$ = 160 milliseconds as true T_2-relaxation times. Signals from 5 different FFs (2%, 5%, 10%, 30%, and 95%) were simulated, each with 20 echoes. The signal amplitude at t = 0 was set to 1.

To study the effect of inaccurate T_2-relaxation times, simulations were performed by using incorrect $T_{2,W}$ and $T_{2,F}$ in the 2-parameter fit method and incorrect $T_{2,F}$ in the 3-parameter fit method. $T_{2,W}$ was set to vary between 22 and 42 milliseconds and $T_{2,F}$ was set to vary between 70 and 260 milliseconds. No noise was added to the signal.

In the Bayesian fitting method, the effect of using an inaccurate S_0 value was studied by varying the S_0 value between 0.8 and 1.2. No noise was added, and each calculation was carried out 1000 times.

The effect of noise was studied in all 3 T_2-based methods by altering the SNR of the simulated signal. The true T_2-relaxation times were used to generate a noise-free signal. Complex Gaussian noise was then added to the signal before calculating the magnitude value. The effect was studied at 5 different SNR levels (20, 50, 150, 300, and 600), defined at t = 0. Each simulation was carried out 1000 times.

RESULTS

Volunteer Study

The estimated mean T_2-relaxation times and standard deviations of muscle (tibialis anterior) and fat (subcutaneous fat), using the monoexponential fit, the 3-parameter fit, and the Bayesian fit are presented in Figure 3. The 3-parameter fit estimated a lower value of $T_{2,W}$ compared with the monoexponential fit and the Bayesian fit. The estimated $T_{2,W}$ from all three methods were independent of matrix size.

Example FF images of all 4 methods can be seen in Figure 4. In contrast to the T_2-based methods, the high-resolution CSEI produced an FF image with a noise level that concealed the anatomy of the calf. Although all 3 T_2-based methods produced FF images in which the different muscles were distinguishable, the estimated FFs were different between the methods. Because the high-resolution CSEI images with a single average (Figure 4) had a low SNR, additional high-resolution MGRE images were acquired with more averages from 1 volunteer (data not shown). Although SNR naturally increased with the number of averages, the noise level was still obscuring the anatomy of the muscles when using 9 averages.

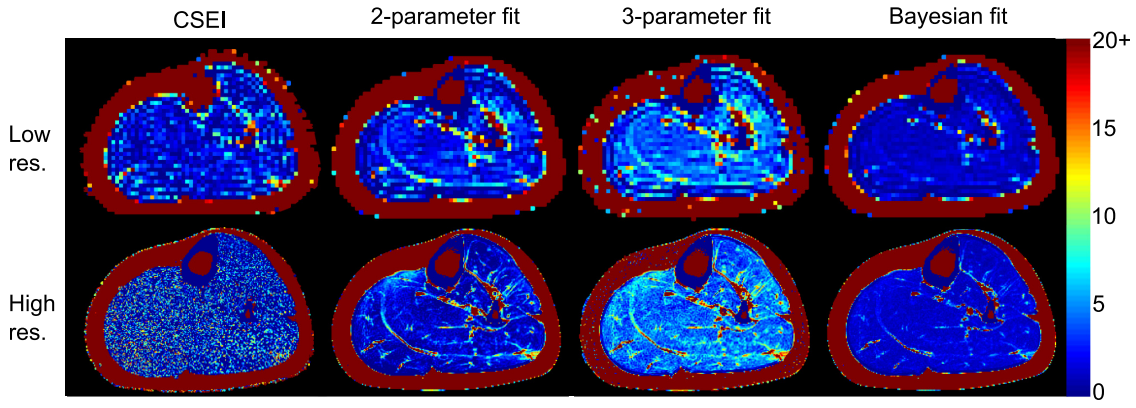

Figure 4. Fat fraction maps of a calf calculated at low and high resolution, using four methods: CSEI, 2-parameter fit, 3-parameter fit, and Bayesian fit.

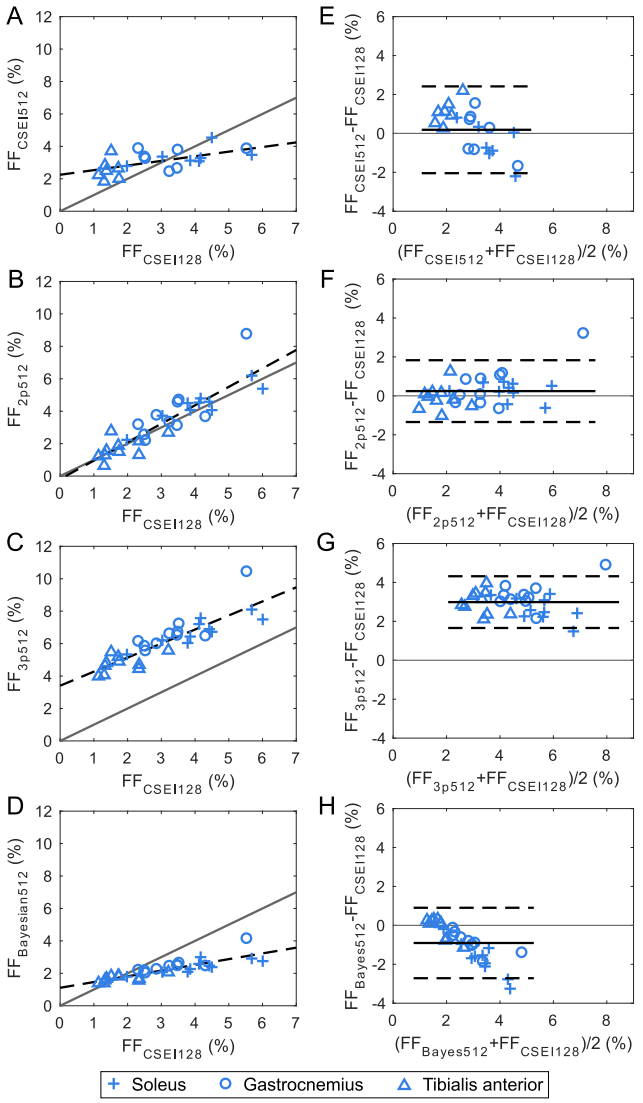

Figure 5. To the left: Scatter plots showing the estimated FF of high-resolution CSEI (A), 2-parameter fit (B), 3-parameter fit (C), and Bayesian fit (D). Each plot shows data points that represent the mean FF within an ROI (3 muscles measured for each volunteer), the linear regression fit (dashed), and the identity line (solid). To the right: Bland–Altman plots of high-resolution CSEI (E), 2-parameter fit (F), 3-parameter fit (G), and Bayesian fit (H), showing the mean difference (solid) and 1.96 standard deviations (dashed).

Scatter plots and Bland–Altman plots of the methods are presented in Figure 5. The linear regression parameters and corresponding confidence intervals are shown in Table 1. Owing to fat–water swaps in the estimated FF images using high-resolution CSEI, results from 3 volunteers were excluded. Compared with the low-resolution CSEI method as reference, the 2-parameter fit was able to estimate the muscle FF accurately, showing only a small overestimation of FFs >3%. High-resolution CSEI overestimated the lower FFs and underestimated the higher FFs of the muscles, whereas the 3-parameter fit consistently overestimated the FF. The Bayesian fitting method showed an underestimation that increased with the FF. In Table 1, the mean values and the standard deviations of the estimated FFs of gastrocnemius, soleus, and tibialis anterior and the corresponding *P*-values of all volunteers and image resolutions are presented. All calculated mean FFs obtained from the 3-parameter fit, at both high and low resolution, significantly ($P < .05$) overestimated the FFs obtained from the reference method in comparison with the 2-parameter fit in which no significant differences were found.

In Figure 6, the acquired signal decay of 3 voxels of low- and high-resolution MESE images and the fitted curves of the 3 T_2-methods are depicted. All 3 methods performed equal at high FF, whereas at lower FFs (~17% and 3%), the estimated signals differ. The 3-parameter fit results in a slower decaying signal compared with the other 2 methods, whereas the Bayesian method results in a faster decaying signal.

The mean SNRs of the single average MESE (second echo)/MGRE (first echo) images of all volunteers were 919/250 (low resolution, muscle), 2048/208 (low resolution, fat), 214/71 (high resolution, muscle), and 449/63 (high resolution, fat). Because the SNR varies over the MESE images owing to parallel imaging, these values represent SNR when the g-factor is close to 1.

Simulations

The simulated effect on the estimation of FF when using incorrect $T_{2,W}$ and $T_{2,F}$, respectively, is shown in Figure 7. In both cases, an underestimation of T_2-relaxation time resulted in an overestimation of the FF, whereas an overestimation of T_2-relaxation time resulted in an underestimation of FF. The 3-parameter fit was more sensitive to errors in $T_{2,F}$ compared with the 2-parameter fit. At higher FFs, it was more important that $T_{2,F}$ was estimated correctly, whereas a correct $T_{2,W}$ was more important at low FFs. For the Bayesian fit, the effect of using an incorrect S_0 value, as well as the standard deviation of the estimated FF, is shown in Figure 8. Using an underestimated S_0 value resulted in an underestimation of the FF, and an overestimated S_0 value resulted in an overestimated FF. However, the effect of using an overestimated S_0 value was greater than that using an underestimated one. Lower FFs (2%–5%) were less sensitive for incorrect S_0 compared with higher FFs (10%–30%). This can also be seen by looking at the standard deviation that was larger for higher FFs.

In Figure 9, the simulated effect of noise is shown as the difference between the estimated and true FFs and the standard deviation of the estimated FF of each of the 3 T_2-based methods. The accuracy of both the 2- and 3-parameter fits increased with SNR (except for FF = 95% using the 3-parameter fit). The 2-parameter fit was less sensitive to noise than the 3-parameter fit. The Bayesian fit was more affected by noise at higher SNR compared with the NLLS-based methods. As the SNR increased, the standard deviation decreased for all methods and FFs.

DISCUSSION

In this work, 3 T_2-based approaches (2-parameter fit, 3-parameter fit, and a Bayesian probability method) have been studied

Table 1. Mean Estimated Fat Fraction and Standard Deviation Between Volunteers, Using All 4 Methods, in Gastrocnemius, Soleus, and Tibialis Anterior Muscles

	CSEI	2-Parameter Fit	3-Parameter Fit	Bayesian Fit
128 × 128				
Fat fraction (%)				
Gastrocnemius	3.39 ± 0.97	2.70 ± 1.95	5.13 ± 1.60	1.99 ± 0.59
	—	($P = 0.43$)	($P = 9.1 \cdot 10^{-3}$)	($P = 1.3 \cdot 10^{-3}$)
Soleus	4.15 ± 1.16	4.48 ± 1.03	6.22 ± 0.98	2.32 ± 0.37
	—	($P = 0.38$)	($P = 1.0 \cdot 10^{-3}$)	($P = 2.2 \cdot 10^{-3}$)
Tibialis anterior	1.80 ± 0.65	1.32 ± 0.67	4.02 ± 0.44	1.5 ± 0.15
	—	($P = 0.19$)	($P = 1.8 \cdot 10^{-4}$)	($P = 0.62$)
Linear regression parameters				
Intercept	—	−0.62	2.1	0.91
		(CI = −1.7–0.45)	(CI = 1.4–2.8)	(CI = 0.65–1.2)
Slope	—	1.1	0.92	0.33
		(CI = 0.78–1.4)	(CI = 0.71–1.1)	(CI = 0.26–0.41)
R^2	—	0.64	0.75	0.74
Bland–Altman				
Mean (limits of agreement)	—	−0.32 (−2.5, 1.9)	1.9 (0.44, 3.3)	−1.2 (−3.0, 0.68)
512 × 512				
Fat fraction (%)				
Gastrocnemius	3.30 ± 0.58	4.00 ± 2.03	6.75 ± 1.52	2.51 ± 0.60
	($P = 0.63$)	($P = 0.52$)	($P = 2.5 \cdot 10^{-4}$)	($P = 9.1 \cdot 10^{-3}$)
Soleus	3.38 ± 0.56	4.42 ± 1.20	6.81 ± 0.95	2.51 ± 0.39
	($P = 0.38$)	($P = 0.43$)	($P = 3.3 \cdot 10^{-4}$)	($P = 2.2 \cdot 10^{-3}$)
Tibialis anterior	2.54 ± 0.62	1.71 ± 0.68	4.79 ± 0.56	1.68 ± 0.21
	($P = 5.8 \cdot 10^{-4}$)	($P = 0.73$)	($P = 1.8 \cdot 10^{-4}$)	($P = 0.68$)
Linear regression parameters				
Intercept	2.2	−0.19	3.4	1.1
	(CI = 1.6–2.9)	(CI = −0.95–0.58)	(CI = 2.8–4.0)	(CI = 0.82–1.4)
Slope	0.29	1.1	0.87	0.35
	(CI = 0.09–0.48)	(CI = 0.91–1.4)	(CI = 0.68–1.1)	(CI = 0.27–0.44)
R^2	0.34	0.79	0.76	0.73
Bland–Altman				
Mean (limits of agreement)	0.18 (−2.0, 2.4)	0.24 (−1.3, 1.8)	3.0 (1.7, 4.3)	−0.91 (−2.7, 0.90)

P-values are given for the comparison against low resolution CSEI. Confidence intervals (CI) are given at a significance level of 0.05.

and compared with CSEI in terms of their capability to correctly estimate low FFs using high-resolution images. This was carried out through a study on healthy volunteers and by simulations. All T_2-based methods provided high-resolution FF images in which it was possible to delineate the different muscles of the calf. With respect to the estimated FFs, the 2-parameter fit showed best agreement to the reference method.

Even though the measured mean FF of high-resolution CSEI in vivo corresponded well with the low-resolution CSEI, the high noise level of the images made it impossible to differentiate any anatomy within the muscle fascia, and therefore, it was difficult to locate potential fat accumulations of the muscles. After acquiring 9 averages, thus increasing SNR, it was still not possible to separate the different muscles of the calf. Using an even larger number of averages to increase SNR further could increase the possibility of differentiating the different muscles groups, but this would result in infeasibly long acquisition times. SNR may also be increased by using a larger flip angle (33). This would, however, require a correction for the T_1-bias, including an estimation of the true flip angle map, and it would therefore introduce an additional source of error. As low-resolution CSEI was used as a reference method, this approach was thus not used. Another way to increase SNR is to acquire 3D MGRE data. In this study, we chose to collect 2D MGRE images for comparison with 2D MESE images. Because only 1 slice was needed, a 2D acquisition allowed for a longer TR and a larger flip angle compared with a 3D acquisition of the same total scan time.

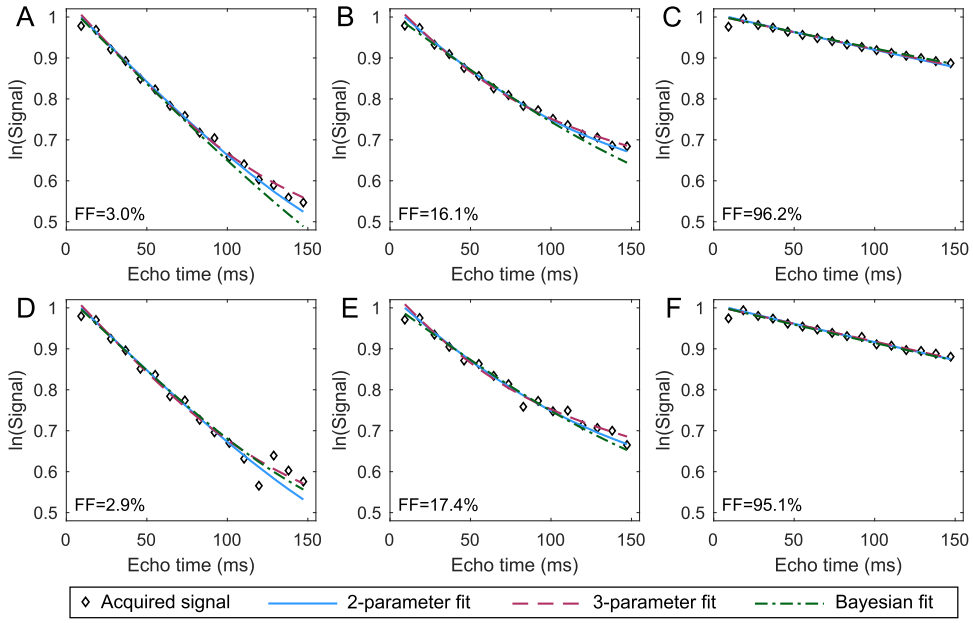

Figure 6. The acquired and fitted signal decay of 3 voxels with different FFs are shown for the low-resolution (A–C) and high-resolution (D–F) MESE images.

Problems with fat–water swaps occurred in some of the estimated FF images of the high-resolution CSEI owing to the long TE needed. All high-resolution CSEI data from 3 subjects had to be excluded because of this. The interecho time of high-resolution CSEI may be reduced by means of bipolar or interleaved data acquisition. However, these approaches are associated with problems with phase errors (28, 34–37). Thus, a single acquisition monopolar readout was chosen to avoid any bias of our reference method.

The estimated T_2-relaxation times of muscle tissue and subcutaneous fat in this study correspond well with T_2-relaxation values of healthy volunteers from literature [$T_{2,W}$ = 32−40 milliseconds and $T_{2,F}$ = 133-154 milliseconds (16, 17, 38–40)], although the Bayesian fitting model results in a slightly overestimated $T_{2,F}$. The measured FFs also agree with previously published data, that is, measured FFs ranging between 1.2% and 3.6% (tibialis anterior), 2.5% and 3.3% (soleus), and 0.91% and 5.0% (gastrocnemius) by using MRI and magnetic resonance spectroscopy fat quantification methods (40–43). Estimation of FF using T_2-based techniques has been conducted in previous studies (17, 18). However, these studies have studied higher FFs (>5%) not comparable with the results of this study.

The importance of high SNR in the estimation of T_2-relaxation times has been studied previously (44). Here, we simulated the effect of noise on fat quantification using T_2-based methods and found that the 2- and 3-parameter fit overestimated the FF at lower SNRs. This could be explained by the fact that the presence of noise might be interpreted by the 3-parameter fit as fat signal, as $T_{2,F} > T_{2,W}$. Using correct T_2-values was also shown to be of importance when using the 2- or 3-parameter fit, particularly for water, to measure low FFs correctly. Owing to a high lowest SNR (~200) of the acquired MESE data, SNR may not be the main issue for the 2- and 3-parameter fit at low and intermediate FFs. Instead, incorrect T_2 values are a more probable cause of bias. Like the NLLS-based methods, the Bayesian fit performed better as SNR increased. Simulations also showed that using a correct S_0 value is important for obtaining an accurate estimation of the FF, particularly for intermediate FFs. The simulated Bayesian fit resulted in a larger standard deviation compared with the NLLS-based methods, suggesting that the Bayesian fitting method, using the *slicesample* algorithm as described in this work, might be less robust. Although this contradicts previous results (25), the used Bayesian probability approaches are not identical and might therefore not be com-

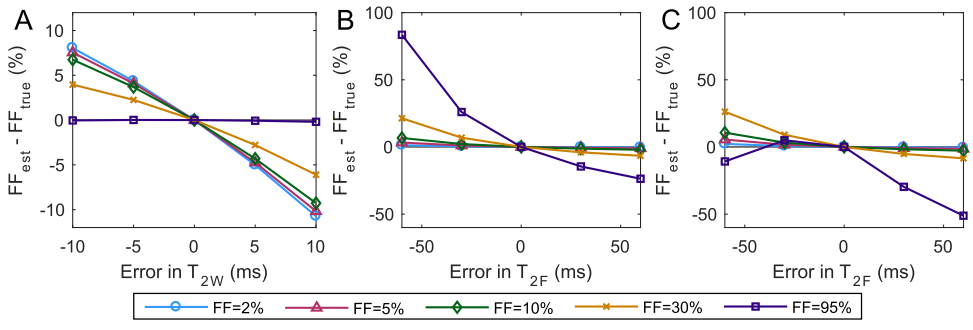

Figure 7. The difference between the true and estimated FFs when using incorrect $T_{2,W}$ (A) and incorrect $T_{2,F}$ (B) in the 2-parameter fit and when using incorrect $T_{2,F}$ (C) in the 3-parameter fit. The true $T_{2,W}$ and $T_{2,F}$ are 40 milliseconds and 160 milliseconds, respectively.

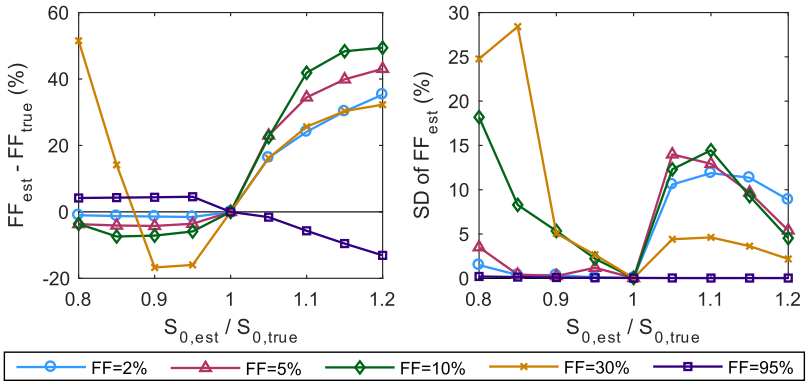

Figure 8. The simulated effect of using an incorrect S_0 value in the Bayesian fitting method showing the difference between the estimated and true FF (left), and the standard deviation of 1000 estimations (right).

parable. In addition, the number of estimated parameters is larger in the Bayesian fit compared with the 2-parameter fit which affects the robustness.

Although the 2-parameter fit resulted in accurate FFs compared with low-resolution CSEI, it depends on whether it is possible to obtain both $T_{2,F}$ and $T_{2,W}$ without any contamination, that is, fluid accumulation due to edema or extramyocellular and intramyocellular fat. It has also been reported that $T_{2,W}$ varies between muscle groups (40). Using a $T_{2,W}$ calculated from an ROI placed in 1 muscle group could therefore result in incorrect FFs in other muscles. In this study, one volunteer had too little available subcutaneous fat, making it impossible to draw a ROI to obtain an individual $T_{2,F}$. Alternatively, one could use T_2-relaxation times obtained from literature. However, simulations in this study suggest that it is important to use correct T_2-relaxation times to avoid biases. A fat quantification method without the need of ROIs, like the Bayesian method, might therefore be preferred.

Owing to varying T_2-values between the muscles, one might expect that keeping $T_{2,W}$ fixed would result in less accurate FF calculation compared with estimating $T_{2,W}$ together with W and F. Both the in vivo results and the simulations suggested that this was not the case, as the 3-parameter fit overestimated the FF, and was more sensitive to incorrect T_2-relaxation times. A recent paper instead described the fat signal decay using a biexponential model, that is, a triexponential model for the total (water and fat) signal (18). It is possible that a biexponential description of the fat signal could improve the results of the NLLS methods in this study. For the Bayesian method, a triexponential signal model has also been studied for intravoxel

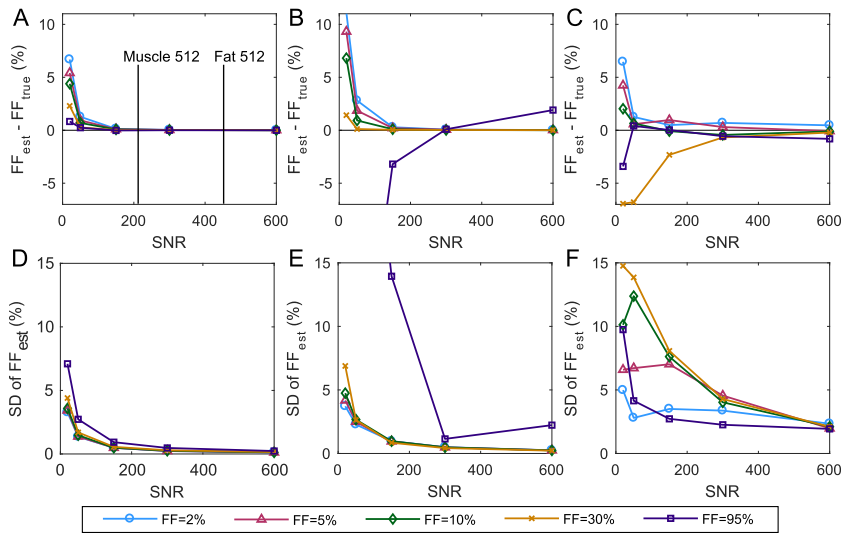

Figure 9. The difference between estimated FF and true FF equal to 2%, 5%, 10%, 30%, and 95% at different signal-to-noise ratios (SNRs) (20, 50, 150, 300, and 600) using the 2-parameter fit (A), the 3-parameter fit (B), and the Bayesian fit (C). The corresponding standard deviations of 1000 estimations using the 2-parameter fit (D), the 3-parameter fit (E), and the Bayesian fit (F) are also shown. The mean SNR of the collected MESE images (512 × 512) in muscle and fat is shown in the first plot (A). At low FF, all 3 methods overestimate the FF in the presence of a high noise level. The difference between estimated and true FF, of the 3-parameter fit outside the shown interval in (B) are: −40.9% (SNR = 20) and −27.8% (SNR = 50). The corresponding standard deviation not shown in (E) is ±41.4% and ±39.0%, respectively.

incoherent motion applications (45), which could be adapted for fat quantification purposes. Another source of error might be the use of only 1 T_2-relaxation time to describe the fat signal decay, although it consists of several composites, each with an individual T_2-relaxation time (29).

Although the Bayesian fit slightly underestimated the FF compared with low-resolution CSEI, there are numerous advantages with the method. For example, all volunteers could be evaluated independent of the amount of subcutaneous fat, as the method is not dependent on the ROI definition. Additional advantages are the possibility of obtaining $T_{2,W}$ maps and that no user input is needed. Further investigations to improve the performance of the Bayesian fit using *slicesample* are needed, including the choice of the number of echoes to include in the calculations, estimation of S_0, smoothing level of the parameter probability density functions, and number of generated samples and burn-in factor in the *slicesample* algorithm.

Several drawbacks with the T_2-based methods that were used in this study were found. First, the effect of B_1-inhomogeneties was not accounted for, assuming perfect T_2 decay of the signal over the course of the MESE acquisition. Methods suggested in previous studies include dismissing voxels where large B_1-inhomogeneites are present by obtaining a B_1-map by an additional data acquisition (18) and using a method based on extended phase graphs (46). Second, owing to the long T_1-relaxation time of muscle tissue, an impractically long TR (>4 seconds) is needed to avoid T_1 bias. Alternatively, as was done here, a T_1-correction can be performed in the postprocessing steps. In this study, T_1-relaxation times obtained from the literature were used to correct for T_1 bias. This can introduce errors if the true T_1-relaxation times are different from the ones obtained from the literature. Using individual T_1-relaxation times could possibly improve the correction, but it will require additional data acquisition. Third, owing to the long acquisition times of MESE images, parallel imaging had to be used to reduce the scan time. This caused varying noise levels and therefore varying SNR over the images.

Several other drawbacks and limitations of the study were identified during this work. The study was conducted in healthy subjects only, and no pathological fat accumulation was seen. Thus, the range of FFs investigated was likely to be lower than that of a patient group. Phantom studies are not included, as it was not possible to construct a phantom which worked for all methods simultaneously. A completely fair comparison of the precision of the various methods was not possible, as they were acquired using different acquisition times and the number of estimated parameters differed between the methods. However, the effect of increasing the acquisition time of high-resolution MGRE images to that of MESE was investigated in 1 subject and it was found to still result in a high noise level and inferior image quality.

In conclusion, all the T_2-based methods could produce high-resolution FF images of the calves of healthy volunteers, where the FF was 1%– 6%. The 2-parameter fit showed the best quantitative agreement to low-resolution CSEI. The method can thus be an alternative to CSEI when the latter method fails to produce high-resolution FF images owing to low SNR or fat–water swaps. However, the NLLS-based methods are sensitive to incorrect T_2-values, particularly $T_{2,W}$ for low FFs. Although the Bayesian fit avoids this particular limitation, further development is needed before it can be used for accurate fat quantification.

ACKNOWLEDGMENTS

This research was supported by Magnus Bergvalls stiftelse and Direktör Albert Påhlssons Stiftelse.

Disclosure: No disclosures to report.

Conflict of Interest: The authors have no conflict of interest to declare.

REFERENCES

1. Karampinos DC, Baum T, Nardo L, Alizai H, Yu H, Carballido-Gamio J, Paran Yap S, Shimakawa A, Link T, Majumdar S. Characterization of the regional distribution of skeletal muscle adipose tissue in type 2 diabetes using chemical shift-based water/fat separation. J Magn Reson Imaging. 2012;35(4):899–907.
2. Nardo L, Karampinos DC, Lansdown DA, Carballido-Gamio J, Lee S, Maroldi R, Ma CB, Link TM, Krug R. Quantitative assessment of fat infiltration in the rotator cuff muscles using water-fat MRI. J Magn Reson Imaging. 2014;39(5):1178–1185.
3. Idilman IS, Aniktar H, Idilman R, Kabacam G, Savas B, Elhan A, Celik A, Bahar K, Karcaaltincaba M. Hepatic steatosis: quantification by proton density fat fraction with MR imaging versus liver biopsy. Radiology. 2013;267(3):767–775.
4. Hu HH, Kim H-W, Nayak KS, Goran MI. Comparison of fat–water MRI and single-voxel MRS in the assessment of hepatic and pancreatic fat fractions in humans. Obesity (Silver Spring). 2010;18(4):841–847.
5. Peterson P, Romu T, Brorson H, Leinhard OD, Mansson S. Fat quantification in skeletal muscle using multigradient-echo imaging: comparison of fat and water references. J Magn Reson Imaging. 2016;43(1):203–212.
6. Goodpaster BH, Thaete FL, Kelley DE. Thigh adipose tissue distribution is associated with insulin resistance in obesity and in type 2 diabetes mellitus. Am J Clin Nutr. 2000;71(4):885–892.
7. Carlier PG, Marty B, Scheidegger O, Loureiro de Sousa P, Baudin P-Y, Snezhko E, Vlodavets D. Skeletal muscle quantitative nuclear magnetic resonance imaging and spectroscopy as an outcome measure for clinical trials. J Neuromuscul Dis. 2016;3(1):1–28.
8. Hocking S, Samocha-Bonet D, Milner K-L, Greenfield JR, Chisholm DJ. Adiposity and insulin resistance in humans: the role of the different tissue and cellular lipid depots. Endocr Rev. 2013;34(4):463–500.
9. Addison O, Marcus RL, Lastayo PC, Ryan AS. Intermuscular fat: a review of the consequences and causes. Int J Endocrinol. 2014;2014:34–36.
10. Damon BM, Li K, Bryant ND. Magnetic resonance imaging of skeletal muscle. Handb Clin Neurol. 2016;136:827–842.
11. Tasca G, Monforte M, Ottaviani P, Pelliccioni M, Frusciante R, Laschena F, Ricci E. Magnetic resonance imaging in a large cohort of facioscapulohumeral muscular dystrophy patients: pattern refinement and implications for clinical trials. Ann Neurol. 2016;79(5):854–864.
12. Torriani M, Townsend E, Thomas BJ, Bredella MA, Ghomi RH, Tseng BS. Lower leg muscle involvement in Duchenne muscular dystrophy: An MR imaging and spectroscopy study. Skeletal Radiol. 2012;41(4):437–445.
13. Friedman SD, Poliachik SL, Carter GT, Budech CB, Bird TD, Shaw DWW. The magnetic resonance imaging spectrum of facioscapulohumeral muscular dystrophy. Muscle Nerve. 2012;45(4):500–506.
14. Mercuri E, Talim B, Moghadaszadeh B, Petit N, Brockington M, Counsell S, Guicheney P, Muntoni F, Merlini L. Clinical and imaging findings in six cases of congenital muscular dystrophy with rigid spine syndrome linked to chromosome 1p (RSMD1). Neuromuscul Disord. 2002;12(7–8):631–638.
15. Meisamy S, Hines CDG, Hamilton G, Sirlin CB, McKenzie C a, Yu H, Brittain JH, Reeder SB. Quantification of hepatic steatosis with T1-independent, T2-corrected

MR imaging with spectral modeling of fat: Blinded comparison with MR spectroscopy. Radiology. 2011;258(3):767–775.
16. Gold GE, Han E, Stainsby J, Wright G, Brittain J, Beaulieu C. Musculoskeletal MRI at 3.0 T: relaxation times and image contrast. AJR Am J Roentgenol. 2004; 183(2):343–351.
17. Kan HE, Scheenen TWJ, Wohlgemuth M, Klomp DWJ, van Loosbroek-Wagenmans I, Padberg GW, Heerschap A. Quantitative MR imaging of individual muscle involvement in facioscapulohumeral muscular dystrophy. Neuromuscul Disord. 2009;19(5):357–362.
18. Azzabou N, Loureiro de Sousa P, Caldas E, Carlier PG. Validation of a generic approach to muscle water T_2 determination at 3T in fat-infiltrated skeletal muscle. J Magn Reson Imaging. 2015;41(3):645–653.
19. Arpan I, Forbes SC, Lott DJ, Senesac CR, Daniels MJ, Triplett WT, Deol JK, Sweeney HL, Walter GA, Vandenborne K. T_2 mapping provides multiple approaches for the characterization of muscle involvement in neuromuscular diseases: a cross-sectional study of lower leg muscles in 5–15-year-old boys with Duchenne muscular dystrophy. NMR Biomed. 2013;26(3):320–328.
20. Månsson S, Peterson P, Johansson E. Quantification of low fat contents: A comparison of MR imaging and spectroscopy methods at 1.5 and 3 T. Magn Reson Imaging. 2012;30(10):1461–1467.
21. Hollingsworth KG, de Sousa PL, Straub V, Carlier PG. Towards harmonization of protocols for MRI outcome measures in skeletal muscle studies: consensus recommendations from two TREAT-NMD NMR workshops, 2 May 2010, Stockholm, Sweden, 1–2 October 2009, Paris, France. Neuromuscul Disord. 2012;22(2): S54–S67.
22. Hu HH, Kan HE. Quantitative proton MR techniques for measuring fat. NMR Biomed. 2013;26(12):1609–1629.
23. Kamman RL, Bakker CJG, Van Dijk P, Stomp GP, Heiner AP, Berendsen HJC. Multi-exponential relaxation analysis with MR imaging and NMR spectroscopy using fat-water systems. Magn Reson Imaging. 1987;5(1):381–392.
24. Bromage GE. A quantification of the hazards of fitting sums of exponentials to noisy data. Comput Phys Commun. 1983;30(3):229–233.
25. Neil JJ, Bretthorst GL. On the use of Bayesian probability theory for analysis of exponential decay data: an example taken from intravoxel incoherent motion experiments. Magn Reson Med. 1993;29(5):642–647.
26. Barbieri S, Donati OF, Froehlich JM, Thoeny HC. Impact of the calculation algorithm on biexponential fitting of diffusion-weighted MRI in upper abdominal organs. Magn Reson Med. 2016;75(5):2175–2184.
27. Kumar D, Nguyen TD, Gauthier SA, Raj A. Bayesian algorithm using spatial priors for multiexponential T_2 relaxometry from multiecho spin echo MRI. Magn Reson Med. 2012;68(5):1536–1543.
28. Yu H, Shimakawa A, Hines CDG, McKenzie CA, Hamilton G, Sirlin CB, Brittain JH, Reeder SB. Combination of complex-based and magnitude-based multiecho water-fat separation for accurate quantification of fat-fraction. Magn Reson Med. 2011;66(1):199–206.
29. Ren J, Dimitrov I, Sherry a D, Malloy CR. Composition of adipose tissue and marrow fat in humans by 1H NMR at 7 Tesla. J Lipid Res. 2008;49(9):2055–2062.
30. Yu H, McKenzie CA, Shimakawa A, Vu AT, Brau ACS, Beatty PJ, Pineda AR, Brittain JH, Reeder SB. Multiecho reconstruction for simultaneous water-fat decomposition and T_2* estimation. J Magn Reson Imaging. 2007;26(4):1153–1161.
31. Bretthorst GL, Hutton WC, Garbow JR, Ackerman JJH. Exponential parameter estimation (in NMR) using Bayesian probability theory. Concepts Magn Reson Part A Bridg Educ Res. 2005;27(2):55–63.
32. Gudbjartsson H, Patz S. The Rician distribution of noisy MRI data. Magn Reson Med. 1995;34(6):910–914.
33. Karampinos DC, Yu H, Shimakawa A, Link TM, Majumdar S. T_1-corrected fat quantification using chemical shift-based water/fat separation: application to skeletal muscle. Magn Reson Med. 2011;66(5):1312–1326.
34. Yu H, Shimakawa A, McKenzie CA, Lu W, Reeder SB, Hinks RS, Brittain JH. Phase and amplitude correction for multi-echo water-fat separation with bipolar acquisitions. J Magn Reson Imaging. 2010;31(5):1264–1271.
35. Ruschke S, Eggers H, Kooijman H, Diefenbach MN, Baum T, Haase A, Rummeny EJ, Hu HH, Karampinos DC. Correction of phase errors in quantitative water-fat imaging using a monopolar time-interleaved multi-echo gradient echo sequence. Magn Reson Med. 2017;78(3):984–996.
36. Peterson P, Månsson S. Fat quantification using multiecho sequences with bipolar gradients: Investigation of accuracy and noise performance. Magn Reson Med. 2014;71(1):219–229.
37. Soliman AS, Wiens CN, Wade TP, McKenzie CA. Fat quantification using an interleaved bipolar acquisition. Magn Reson Med. 2016;75(5):2000–2008.
38. Pai A, Li X, Majumdar S. A comparative study at 3 T of sequence dependence of T_2 quantitation in the knee. Magn Reson Imaging. 2008;26(9):1215–1220.
39. Gloor M, Fasler S, Fischmann A, Haas T, Bieri O, Heinimann K, Wetzel SG, Scheffler K, Fischer D. Quantification of fat infiltration in oculopharyngeal muscular dystrophy: Comparison of three MR imaging methods. J Magn Reson Imaging. 2011;33(1):203–210.
40. Schwenzer NF, Martirosian P, Machann J, Schraml C, Steidle G, Claussen CD, Schick F. Aging effects on human calf muscle properties assessed by MRI at 3 Tesla. J Magn Reson Imaging. 2009;29(6):1346–1354.
41. Schick F, Machann J, Brechtel K, Strempfer A, Klumpp B, Stein DT, Jacob S. MRI of muscular fat. Magn Reson Med. 2002;47(4):720–727.
42. Machann J, Bachmann OP, Brechtel K, Dahl DB, Wietek B, Klumpp B, Häring HU, Claussen CD, Jacob S, Schick F. Lipid content in the musculature of the lower leg assessed by fat selective MRI: intra- and interindividual differences and correlation with anthropometric and metabolic data. J Magn Reson Imaging. 2003;17(3):350–357.
43. Fischer MA, Pfirrmann CW, Espinosa N, Raptis DA, Buck FM. Dixon-based MRI for assessment of muscle-fat content in phantoms, healthy volunteers and patients with achillodynia: comparison to visual assessment of calf muscle quality. Eur Radiol. 2014;24(6):1366–1375.
44. Raya JG, Dietrich O, Horng A, Weber J, Reiser MF, Glaser C. T_2 measurement in articular cartilage: impact of the fitting method on accuracy and precision at low SNR. Magn Reson Med. 2010;63(1):181–193.
45. Ohno N, Miyati T, Kobayashi S, Gabata T. Modified triexponential analysis of intravoxel incoherent motion for brain perfusion and diffusion. J Magn Reson Imaging. 2016;43(4):818–823.
46. Marty B, Baudin PY, Reyngoudt H, Azzabou N, Araujo ECA, Carlier PG, de Sousa PL. Simultaneous muscle water T_2 and fat fraction mapping using transverse relaxometry with stimulated echo compensation. NMR Biomed. 2016;29: 431–443.